Available online at www.sciencedirect.com
ScienceDirect
Bioelectrochemistry 71 (2007) 223–232
Bioelectrochemistry
www.elsevier.com/locate/bioelechem

Ion transport in tumors under electrochemical treatment: In vivo, in vitro and in silico modeling

L. Colombo [a], G. González [b], G. Marshall [b,*], F.V. Molina [c], A. Soba [b], C. Suarez [b], P. Turjanski [b]

[a] Depto. de Inmunobiología, Inst. de Oncología Angel H. Roffo, Universidad de Buenos Aires, (C1417DTB) Buenos Aires, Argentina
[b] Laboratorio de Sistemas Complejos, Departamento de Computación, FCEyN, Universidad de Buenos Aires, (C1428EGA) Buenos Aires, Argentina
[c] INQUIMAE, FCEyN, Universidad de Buenos Aires, (C1428EHA) Buenos Aires, Argentina

Received 12 September 2006; received in revised form 14 June 2007; accepted 6 July 2007
Available online 13 July 2007

Abstract

The electrochemical treatment of cancer (EChT) consists in the passage of a direct electric current through two or more electrodes inserted locally in the tumor tissue. The extreme pH changes induced have been proposed as the main tumor destruction mechanism. Here, we study ion transport during EChT through a combined modeling methodology: in vivo modeling with BALB/c mice bearing a subcutaneous tumor, in vitro modeling with agar and collagen gels, and in silico modeling using the one-dimensional Nernst–Planck and Poisson equations for ion transport in a four-ion electrolyte. This combined modeling approach reveals that, under EChT modeling, an initial condition with almost neutral pH evolves between electrodes into extreme cathodic alkaline and anodic acidic fronts moving towards each other, leaving the possible existence of a biological pH region between them; towards the periphery, the pH decays to its neutral values. pH front tracking unveils a time scaling close to $t^{1/2}$, signature of a diffusion-controlled process. These results could have significant implications in EChT optimal operative conditions and dose planning, in particular, in the way in which the evolving EChT pH region covers the active cancer cells spherical casket.

Keywords: Tumors; Computational modeling; Electrochemical treatment; Ion transport

1. Introduction

In electrochemical treatment (EChT) therapy a direct electric current flows through the tumor cellular and interstitial compartments, the latter consisting mainly in a complex conglomerate of collagen, glycoproteins, proteoglycans and hyaluronic acid. Tissue destruction has been reported by this technique in a wide range of solid tumors, with greater efficacy observed in skin cancer, oral cavity and thyroid malignancies [1]. Although known since the end of the 19th century, Bjorn Nordenstrom, from Sweden, is considered to be a pioneer in the treatment of tumors with electric current and combination therapies in patients [2,3]. In the late seventies, Nordenstrom treated primary lung cancers by applying current between two platinum wire electrodes and, in his book of 1983 [2], he reported results from the treatment of 26 lung tumors in 20 patients. Regression was obtained in 12 out of 26 tumors and no signs of regrowth were detected after a 2–5 year follow-up period.

Following Nordenstrom works, Xin Yu-Ling and his group in China extended EChT to the whole country (more than 15000 patients have been treated in the last 15 years) [4,5]. Miklavcic and collaborators in Slovenia, in a series of papers starting in 1991, studied the effects of EChT on tumors in mice [6–9]. In particular, Sersa et al. [10] studied the potentiated effects of EChT when combined with anticancer drugs such as bleomycin. More recently, von Euler et al. [11] presented results of cell proliferation and apoptosis in rat mammary cancer after EChT treatment. At present, there are several groups working in Australia, Cuba, Japan, Sweden and the USA; a general review can be found in Nilsson et al. [1]. Some of the advantages of EChT are its simplicity, effectiveness, low cost and negligible side effects. This therapy is specially indicated for superficial, not-operable or chemotherapy-resistant tumors. It has also been suggested that the EChT would potentiate the antineoplasic effects of radio and chemotherapy and minimize their side effects [3,12–14].

* Corresponding author. Tel.: +54 11 4576 3390x709; fax: +54 11 4576 3359.
E-mail address: marshallg@arnet.com.ar (G. Marshall).

1567-5394/$ - see front matter © 2007 Elsevier B.V. All rights reserved.
doi:10.1016/j.bioelechem.2007.07.001

The induced transmembrane voltage in a cell subject to an electric field results in an increase in membrane permeability, thus allowing certain molecules to be transported into the cell [15]. This process is usually called electroporation or electropermeabilization and has been widely used in molecular biology and related fields. Electrochemotherapy (ECT) is a more recent technique based on cell electropermeabilization combined with the use of chemotherapy thus allowing greater therapy efficiency as much more drug can penetrate the cell (it is used specially with effective drugs such as bleomycin or cisplatin but with low membrane permeability). A review can be found in the European Journal of Cancer Supplements, 2006, Volume 4, edited by L. Mir. Pioneering studies of ECT were presented in 1991 by Mir et al. [16] from the Institute Gustave Roussy, Villejuif; their work stimulated other groups, among them, Miklavcic et al. [17] from the Institute of Oncology, Ljubljana, Slovenia. To date more than 200 patients with tumor nodules were treated with ECT using as anticancer drug bleomycin or cisplatin. The majority of patients had melanoma metastases, followed by patients with metastases of skin, head and neck, mammary, ovarian cancer, Kaposi's sarcoma and chondrosarcoma. The results of the treatment showed good antitumor effectiveness, resulting in approximately 80% objective responses of the treated tumor nodules. In fact, ECT being an easy, highly effective and safe anticancer therapy is becoming a standard treatment for cutaneous and subcutaneous tumor nodules, mainly as a palliative, but further progress in the development of new electrodes will no doubt extend its use as an effective tumor ablation technique [18].

In the present work we will focus on the EChT technique, specifically on ion transport. It is expected that many of the results of this study will serve in the near future to study fundamental aspects of ion transport during ECT or a combination of EChT and ECT.

Experimental observations in EChT show that the electric field causes a flux of interstitial water from anode to cathode. Tissue surrounding the anode dehydrates and edema results at the cathode. Hydroxyl ions and hydrogen gas are liberated at the cathode while hydrogen ions, oxygen and chlorine gas are produced at the anode. These reactions induce an important pH change (acidic at the anode and alkaline at the cathode). It is generally agreed that this pH change is the main tumor destruction mechanism through necrosis and apoptosis inducement [11].

Although the experience gained in China, the destructive mechanisms involved in EChT are still not well known. Thus, it is necessary to have a better understanding of the fundamental mechanisms involved in its action and to elaborate a reliable strategy for dosage optimization. With this goal in mind, here we propose a triple combined methodology for studying EChT in tumors: in vivo, in vitro and in silico modeling (VVS). We believe VVS to be a powerful tool permitting a complementary and thus richer multidisciplinary view of this complex problem while assuring that experimental and/or numerical artifacts are more easily detected.

In the in vivo EChT modeling of a human tumor we deal with a solid tumor developed subcutaneously in mice subject to an electric field. Animal models have been invaluable in the study of human cancer. One of the main reasons is that mouse and humans have roughly the same complement of genes and signal pathways (tumors in mouse and humans mutate in the same class of genes which is an index of similar mechanisms governing tumor growth). In fact, literature shows that mice are potentially useful in the establishment of better preclinical modeling [19].

In the in vitro EChT modeling of a human tumor we use a gel of collagen I subject to an electric field where it is assumed that the gel has physicochemical and hydrodynamic properties close to those found in the interstitium of a solid tumor. The use of collagen is based upon the fact that it constitutes more than 70% of the tumor interstitium. Moreover, previous evidence indicates that collagen type I gels may be a good initial simplified model of the transport of species in the tumor extracellular matrix [20,21]. We also use a gel of agar, because it is more suitable for optical studies and more chemically resistant.

In silico or numerical cancer modeling is a powerful tool that can provide more insight into the mechanisms that control tumor evolution and growth. It implies both mathematical modeling and numerical simulation. In general it consists in a system of reaction-transport differential equations in a fixed or moving domain (Stefan-like problem) describing physicochemical conservation laws whose solution is obtained through numerical methods. At present it is an active area of research and a review can be found in the book of Preziosi [22]. Pioneering work in the subject was done by Jain and his group from the Steele Laboratory, Department of Radiation Oncology, Massachusetts General Hospital and Harvard Medical School, Boston, USA ([23–26]).

EChT in silico modeling was pioneered by Nilsson and coworkers in Sweden in a series of papers [27–30]. They described ion transport in a zone near one of the electrodes (cathode or anode) by a quasi one-dimensional model using the Nernst–Planck equations for ion transport under the hypothesis of electroneutrality. In their first model the tissue matrix was approximated to a saline (NaCl) solution with a determined buffer capacity and organic content.

In successive refinements the model was extended to include the bicarbonate buffer effects on anodic hydrogen ions and the transport and reaction of chlorine and chlorinated species. The results were compared with experimental data from in vivo rat normal tissue giving a good description of the pH profile near the anode after EChT. In their last model [30], they studied ion transport near the cathode in which they show their simulated pH profiles to be strongly correlated with the size of experimentally measured lesions, thus confirming that the spreading of hydroxyl ions determines the size of the lesion around the cathode. They also suggested that the model could be used for predicting the size of the lesion produced by EChT.

The study of ion transport in electrodeposition in thin layer cells (ECD) has many analogies with EChT that can be exploited to advance in our knowledge of EChT. In ECD the electrolytic cell consists of two microscope slides sandwiching two parallel electrodes and an electrolyte. A voltage difference applied between electrodes produces ramified deposits with complex geometries ranging from fractal to dense branching [31–37].

Based on our previous knowledge in ECD [31–37], here we introduce an EChT in silico tumor modeling consisting in the one-dimensional Nernst–Planck equations for ion transport in a four component electrolyte (Na^+, OH^-, Cl^- and H^+) and the Poisson equation for the electrostatic potential under galvanostatic conditions. Since no electroneutrality condition is imposed and the full cathode–anode ion transport interaction is taken into account, our model appears to give a better description of EChT than previously published models.

In summary, the general goal of this paper is to develop a quantitative understanding of ion transport in EChT through a VVS strategy, in which experimental results are integrated into a unified macroscopic mathematical model. We believe that simulations with this model could help to achieve a better understanding of tumor ion transport and aid in the development of optimal strategies for improved cancer treatment.

The plan of the paper follows: Section 2 presents in vivo modeling with mice, Section 3 describes in vitro modeling with gels of agar and collagen, Section 4 introduces the in silico modeling and simulations, and finally, Sections 5 and 6 present a discussion and conclusions, respectively.

2. In vivo experiments

The in vivo EChT modeling consists in the study of subcutaneous tumors in mice treated with three different Coulomb dosages of EChT. Tissue destruction and pH profiles in tissue near one of the electrodes are measured.

2.1. Methods

We used 3–4 month old tumor-bearing BALB/c male mice from the Instituto de Oncología Angel H. Roffo. Animals were maintained in accordance with ethics, current regulations and standards of the NIH. The mammary adenocarcinoma M2 appeared spontaneously in BALB/c female mouse and is maintained by successive subcutaneous in vivo implants into the flank of syngeneic mice. This kind of tumor is well characterized and has relatively low necrosis development and metastatic ability. Subcutaneous tumors (in vivo passage 137 to 141) were subjected to EChT when their size reached an area of approximately 1.5 cm^2.

To study the size of the necrotic area of the tissue after EChT, as a function of the Coulomb dosage, animals were randomly divided into 3 groups, each one treated, under general anesthesia (ip Ketamine–Silacine solution, 0.01 ml/g) with different Coulomb (C) dosages of a direct electric current: 10 C (10 mA, 17 min), 30 C (17 mA, 29 min) and 50 C (20 mA, 42 min). These dosages were chosen based upon previous published data [14]. A punctual platinum electrode (anode) with a diameter of 1 mm was inserted in the centre of the tumor in a caudal–cranial direction while the cathode was placed subcutaneously far away from it. Direct electric current was applied with a power supply (Consort E835, Belgium). Both current and voltage were continuously monitored. To avoid muscle twitching, linear current ramps with a length of 2 min were applied at the beginning of the treatment.

After EChT, mice were euthanized and the tumor was longitudinally cleaved in half, along the electrode insertion plane. The macroscopic necrotic area, defined by a dark, almost spherical colored zone around the electrode, was measured along the longitudinal axis of the tumor.

To study the spatial pH profiles after EChT, results were taken over 5 experiments with 3 mice per group in each one (total: $3\times5=15$ mice per group). Following identical procedures as previously described, pH measurements were made between 5 to 10 min after current shutdown with a microcombination electrode with a tip diameter of 1.5 mm (PHR-146, Lazar Research Lab, Inc., Ca). Values were taken every 2 mm along radial directions, from the centre of the tumor (where the anode had been placed), towards the periphery and even into the healthy tissue.

2.2. Results

Results of the size of the anodic necrotic area, defined by the diameter of an almost spherical colored zone near the anode, are presented in Fig. 1. They reveal that the macroscopic necrotic area around the anode, scales linearly with the Coulomb dosage. An ANOVA statistical analysis of repeated measurements revealed significative differences between dosages. Specifically, Tukeys test for post-hoc comparisons showed that the 50 C dosage is significative different from 10 C and 30 C dosages ($11.46+3.2$ and $17.5+3.2$ mm for 10 and 30 C respectively, $p=0.0002$). Dark brown zones were observed that are attributed to the formation of acid and basic heamatin [38]. The color patterns of the lesions are in agreement with results found in other studies [39]. Water transport, from the anode to the cathode, also caused a severe dehydration in tissue around the anode and a prominent oedema at the cathode. At the highest dose, it was also observed the formation of a subcutaneous combustible gas bubble probably consisting of an accumulation of hydrogen gas originated at the cathode.

Fig. 2 shows the spatial pH profiles obtained. They reveal the medium to be very acidic at the anode and rising away towards tumor periphery where it reaches fairly neutral values. Extreme pH values near the anode should be taken with caution and considered only qualitatively since they are out of the dynamic range of the meter. An ANOVA statistical analysis of repeated

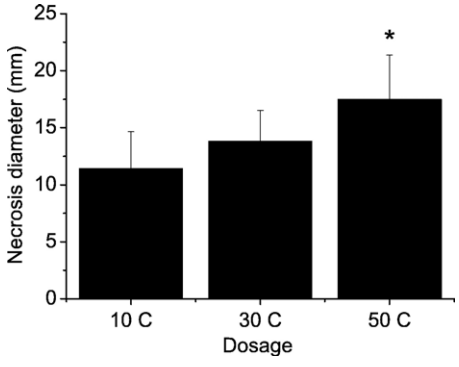

Fig. 1. Anodic necrosis diameters for different Coulomb dosages (10, 30 and 50 C); $p<0.05$.

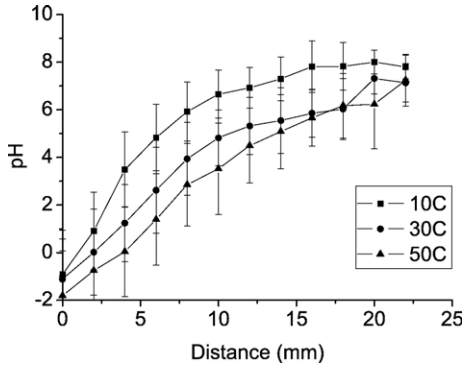

Fig. 2. Spatial pH profiles in tumors vs distance anode–periphery for different Coulomb dosages.

measurements showed that spatial pH differences are significant ($p < 0.00001$) but differences between dosages are not ($p = 0.08$).

3. In vitro experiments

In vitro modeling is based in the application of the EChT at different current and Coulomb dosages to collagen type I gels and to agar gels and the measurement of the resultant pH profiles in space and time.

3.1. Methods

For EChT collagen gel measurements, a collagen type I was diluted in distilled water at 2 different concentrations (30 mg/ml and 50 mg/ml) and allowed to become a gel. Both concentrations were chosen so as to simulate the basic composition of the extracellular matrix of tumors of different consistency as it has been observed that it can range from denser ones (e.g. subcutaneous tumors) to softer ones (e.g. brain tumors) [40]. It has also been described that collagen content would be the main component responsible for determining the consistency level [20]. In the EChT application, three different Coulomb dosages were used: 3 C (10 mA, 5 min), 10 C (10 mA, 17 min) and 30 C (17 mA, 29 min). Two platinum punctual electrodes, with a tip diameter of 1 mm, were inserted in the gel with a separation of 3 cm between them. Direct electric current was applied with a power supply. Both current and voltage were continuously monitored. pH measurements in the gel at the end of the treatment were taken every 2 mm, by means of the microcombination electrode previously described, along a line between both electrodes and away from them into the periphery.

For EChT agar–agar gel measurements, a gel dehydrated for microbiological use in a concentration of 1 g/100 ml was used. NaCl was added in a final concentration of 1 mM and phenolphthalein ($C_{20}H_{14}O_4$) was used as an acid–base indicator. From the resulting solution a 0.26 cm thick film was made. Platinum punctual electrodes, 1 mm in diameter, submerged 2 mm into the gel and separated 4 cm, were employed. pH front tracking was done with an optical absorption technique described in [34]. In this particular case, the pH 8–9 isoline corresponded to the phenolphthalein color change. Illumination was done through an adequate high intensity led with wave length emission near the maximum absorption of the indicator basic form (374 nm). Video camera images were captured at 0.2 frame/s with a resolution of 455 pixels/cm.

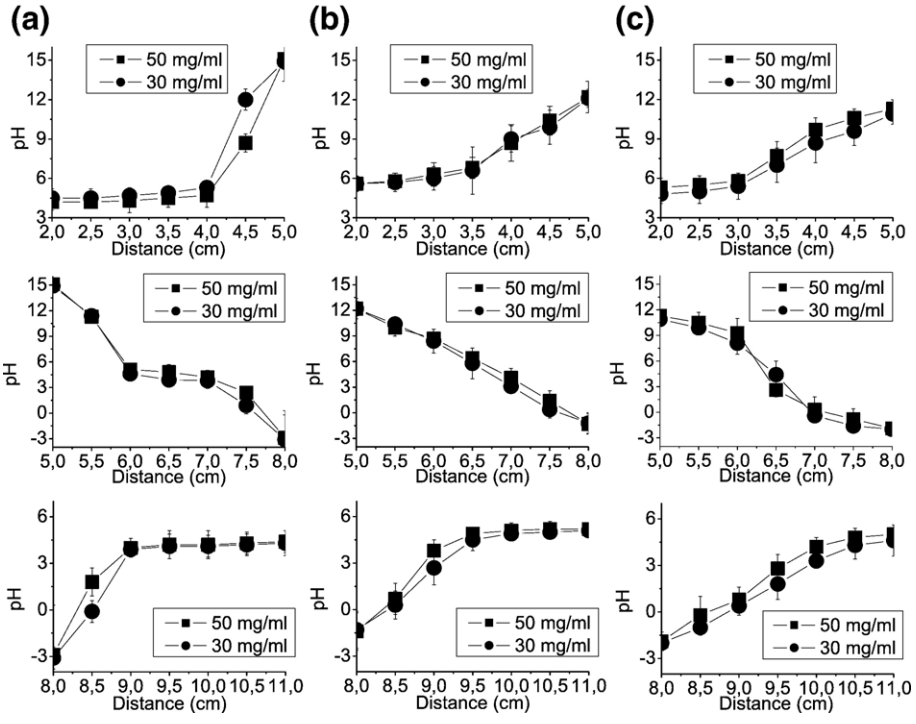

Fig. 3. EChT collagen gel modeling pH profiles vs distance for different Coulomb dosages (3, 10 and 30 C) in a type I collagen gel with different concentrations (50 and 30 mg/ml). (a): 3 C, (b): 10 C, and (c): 30 C. Left column: periphery–cathode distance; central column: cathode–anode distance; right column: anode–periphery distance.

3.2. Results

EChT collagen gel measurements obtained from four independent experiments are presented in Fig. 3. An ANOVA statistical analysis of repeated measurements showed that spatial pH differences between different regions and dosages are significative ($p < 0.00001$ and $p = 0.0001$ respectively) though there are not significative differences between gel concentrations. As expected, there is a shift towards an expansion of the basic area around the cathode (Fig. 3, left column) and of the acidic area around the anode (Fig. 3, right column) as the Coulomb dosage increases (larger current implies larger voltage and thus larger front propagation speed). As a consequence of this, the pH profile in zones near both electrodes shows rather smoother slopes as the Coulomb dosage increases. Again, extreme pH values near the electrodes should be taken with caution and considered only qualitatively since they are out of the dynamic range of the meter. We also report a cathode–anode pH profile that changes significantly between dosages (Fig. 3, central column), with the lower ones presenting an intermediate region of near neutral pH which disappears at the higher dosage. This corresponds to the gradual expansion of pH fronts emerging from each electrode up to the moment of their encounter. The pH value at the periphery is around five rather than seven because gels were made with water in equilibrium with air. A denaturalization of the collagen near both electrodes was also observed, which is consistent with the extreme pH values found at those points.

For EChT agar gel modeling, Fig. 4 shows snapshots at different times of the alkaline cathodic almost spherical region (visualized as dark pixels with the cathode at its center) taken at 75, 150, 225 and 300 s. Images have been enhanced with the acid–base indicator, an optical absorption technique and a further image post-processing. The border of these regions (a rather thin transition layer) may be taken as a constant pH line corresponding to the phenolphtalein indicator transition (pH = 8.5, approximately).

Fig. 5a shows the pH 8–9 isoline front tracking in time in a logarithmic scale for different electric current densities (taken from experiments similar to the one shown in Fig. 4). This figure reveals that for increasing times the pH front scales in time as $t^{0.58}$, $t^{0.51}$, y $t^{0.57}$ respectively for different electric current densities. These are close to $t^{1/2}$, which is characteristic of diffusive transport, indicating that convection is almost suppressed by the high viscosity of the gel employed. The transport of OH^- ions is diffusive because current transport is mainly done by the support electrolyte (NaCl).

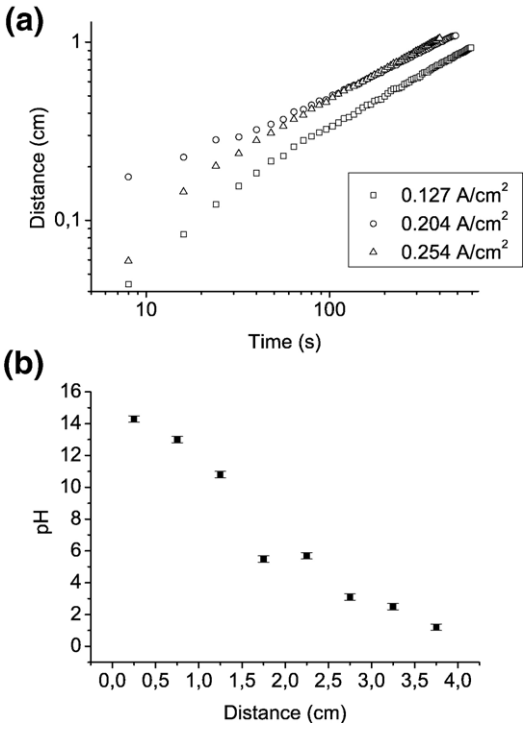

Fig. 5. pH 8–9 isoline front tracking evolution in time in a logarithmic scale (a); cathode–anode pH variation at $t = 600$ s and 10 mA (b).

Fig. 5 shows pH measurements between cathode and anode made 600 s after applying the EChT (10 mA). The pH was measured using the micro-combination electrode previously described. This figure unveils the presence of a pH plateau in the middle of the distance cathode–anode showing the situation previous to the mixing of a cathodic alkaline pH front with an acidic anodic depletion acidic front.

Fig. 6 shows the time evolution of the electrostatic potential in the cell for different electric current densities obtained with experiments similar to those presented in Fig. 5. These results reveal that the cell resistance decreases in time, the main cause being the generation of H^+ and OH^- ions at the electrodes. In a similar fashion to previous experiments, Fig. 6(b) shows the Cl_2 front of an experiment in which the Cl_2 generated from the anodic reaction of Cl^- and solubilized in the medium is tracked using *o*-toluidine as a colorimetric indicator. This figure reveals

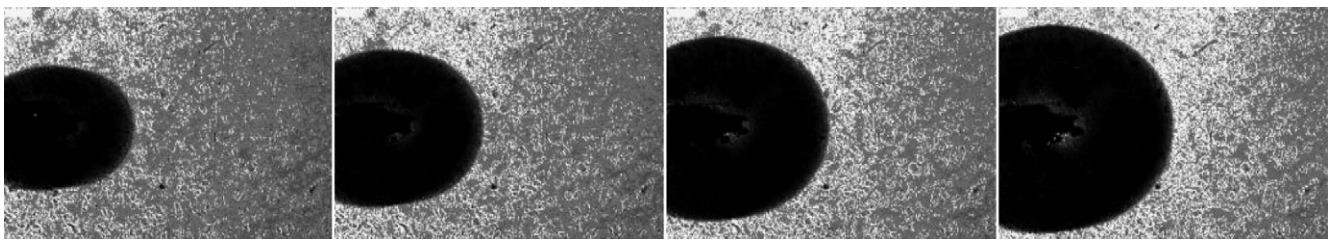

Fig. 4. EChT agar gel modeling showing snapshots of the cathodic alkaline almost spherical region (visualized as dark pixels) with the cathode at its center, taken at 75, 150, 225 and 300 s. Experiments done at 5 mA and the image size is 1.1 cm × 1.5 cm.

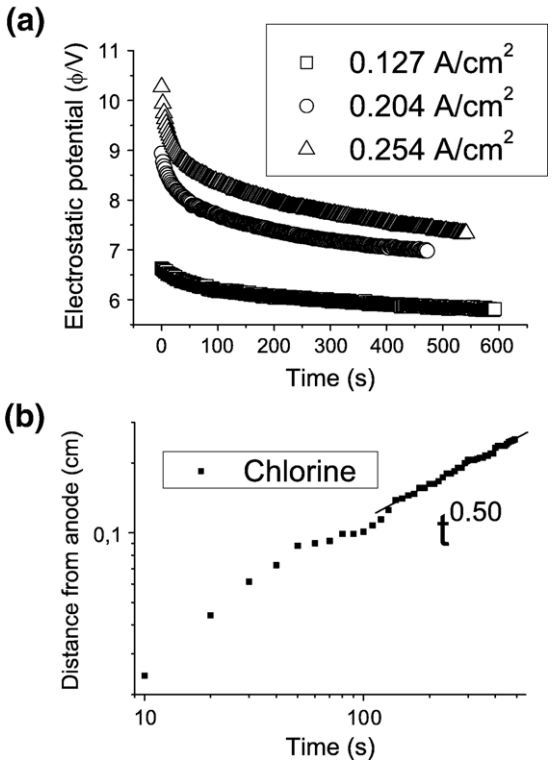

Fig. 6. electrostatic potential in the cell vs time for different current densities (a); Cl_2 anodic front tracking (b).

as expected that the front scales in time as $t^{0.5}$ showing the diffusive character of the Cl_2 front.

4. In silico modeling

4.1. Mathematical method

The physical model is described by the mass conservation law, the Nernst–Planck equations for the concentration of the ions subject to diffusion and migration fields, and the Poisson equation for the electrostatic potential. They are respectively [31]:

$$\frac{\partial C_i}{\partial t} = -\nabla \cdot J_i \tag{1}$$

$$J_i = -\mu_i C_i \nabla \phi - D_i \nabla C_i \tag{2}$$

$$\nabla^2 \phi = -\frac{F}{\epsilon} \sum_i z_i C_i. \tag{3}$$

Here ϕ is the electrostatic potential, C_i is the concentration of the ionic species i, where $i = Na^+$, OH^-, Cl^- and H^+ ions; J_i, is the flux of the ionic species i (moles passing through a unit of area per unity time). z_i and D_i are charge number, and the diffusion coefficient of the species i; $\mu i = z_i\, D_i F/RT$ being its respective (signed) mobilities and ϵ is the absolute medium permittivity, with F the Faraday constant, R the gas constant and T the absolute temperature. z_i are signed quantities, being positive for cations and negative for anions; e is the electronic charge, and ε is the permittivity of the medium.

Through a dimensional analysis it is possible to write the previous system in the following form

$$\frac{\partial C_i^*}{\partial t^*} = -\nabla \cdot J_i^* \tag{4}$$

$$J_i^* = -M_i C_i^* \nabla \phi^* - \frac{1}{Pe_i} \nabla C_i^* \tag{5}$$

$$\nabla^2 \phi^* = Po \sum_i z_i C_i^* . \tag{6}$$

Here $\phi^* = \phi/\phi_0$ is a dimensionless electrostatic potential, $C_i^* = C_i/C_0$ is the dimensionless concentration of the ionic species i, and $J_i^* = J_i/J_0$, is the dimensionless flux of the ionic species i. The quantities $M_i = y_0^2/t_0\phi_0\mu_i$, $Pe_i = y_0^2/t_0 D_i$ and $Po = \epsilon\phi_0/x_0^2 C_0 e$ stand for the dimensionless numbers Migration, Peclet and Electric Poisson, respectively. y_0, t_0, ϕ_0, C_0 and J_0 are reference values for the length, time, electrostatic potential, concentration and flux, respectively (see details in [37]).

Details of the boundary conditions for EChT under constant electric current conditions as well as a discussion of dimensionless numbers, can be found in [37]. In what follows, for convenience, we drop the asterisk in the dimensionless quantities of previous equations. Typical experimental values of the dimensionless numbers in a cell with $L = 3$ cm, $d = 0.05$ cm, $C = 0.1$ M and $I = 10$ mA result in: $M_C = 22\,000$, $M_A = 14\,000$, $M_{H^+} = 3000$, $M_{OH^-} = 5500$, $Pe_C = 7.5E5$, $Pe_A = 5E5$, $Pe_{H^+} = 2.0E5$, $Pe_{OH^-} = 1.0E5$ and $Po = 0.44$ [37]. The range of values of the dimensionless numbers reflects the disparity of scales of the processes involved in ECD [37] yielding a stiff numerical problem.

The one-dimensional system was solved, for each time step, in a fixed domain on a two-dimensional space–time uniform lattice using finite differences and deterministic relaxation techniques, under galvanostatic conditions (see [37] for details). The computational model was written in the C language and implemented on a Pentium class computer under Windows XP. All the results are plotted in dimensionless form.

In the numerical simulations presented below we used a four-component electrolyte under galvanostatic conditions, and the fluid viscosity is taken into consideration through the values of

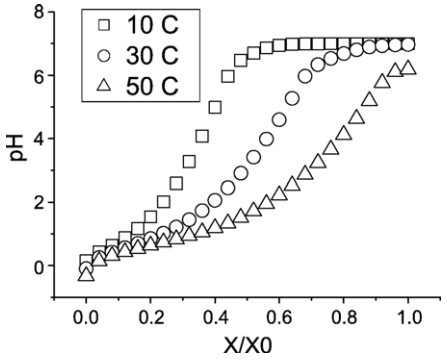

Fig. 7. Simulated pH profiles vs distance anode–periphery (indicated by x) for different Coulomb dosages ($x_0 = 3$ cm).

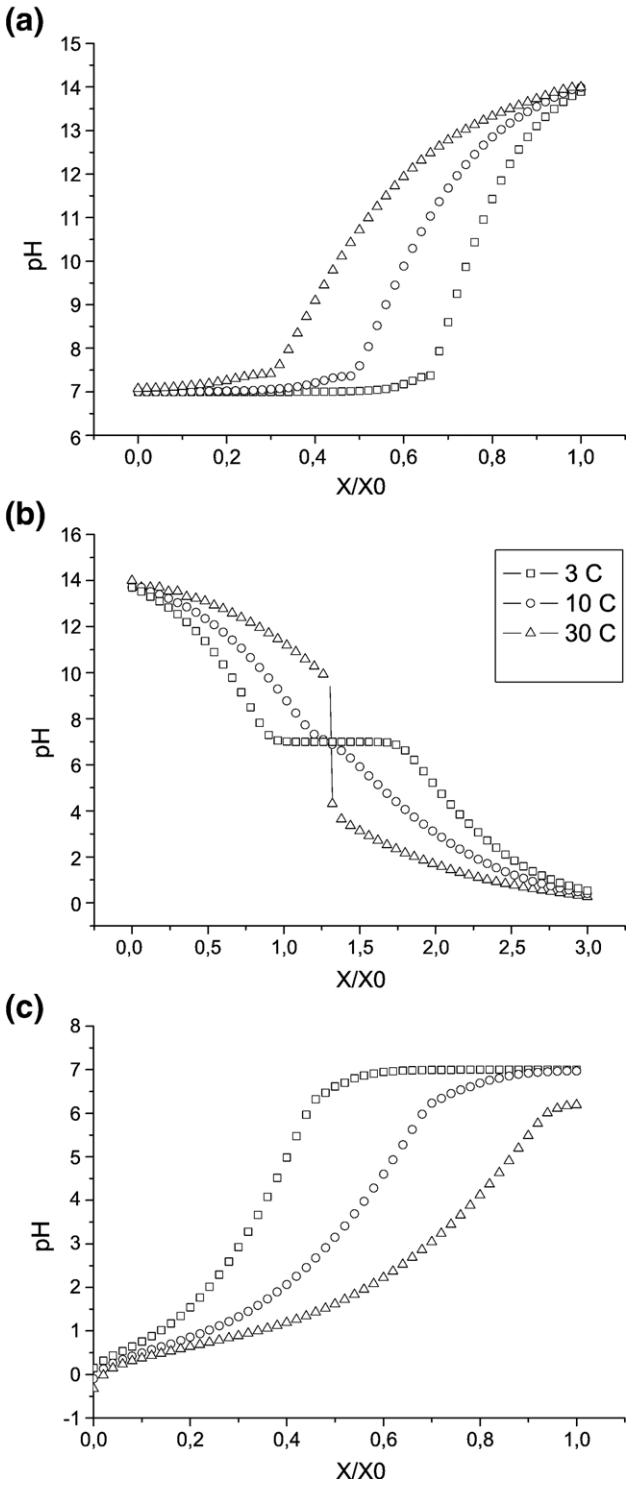

Fig. 8. Simulated pH profiles vs distance: periphery–cathode (a), cathode–anode (b), and anode–periphery (c), for different Coulomb dosages (x_0=3 cm).

the diffusion and mobility coefficients. The disparity of scales of the processes being simulated precludes the use of some of the real dimensionless numbers. In this context, the initial dimension less conditions at t=0 are $C_{Na}=C_{Cl}=1.0$ and $C_H=C_{OH}=10^{-7}$ and a ramp function between cathode and anode for the electrostatic potential.

4.2. Numerical results

Fig. 7 shows in silico pH profiles vs distance from the anode to the periphery, for different Coulomb dosages (10 C (10 mA, 17 min), 30 C (17 mA, 29 min) and 50 C (20 mA, 42 min)). Extreme acidic values can be observed at the anode while almost neutral ones appear at the periphery. These results are well correlated with in vivo results from Fig. 2.

Fig. 8 shows in silico pH profiles vs distance (periphery–cathode, cathode–anode and anode–periphery, respectively), for different Coulomb dosages (3 C (10 mA, 5 min), 10 C (10 mA, 17 min), and 30 C (17 mA, 29 min)). Comparison with in vitro collagen measurements from Fig. 3 reveals that pH variations are well correlated: almost neutral values at the periphery, extreme alkaline values at the cathode and extreme acidic values at the anode. The pH variation between cathode and anode are also well correlated for some of the dosages. Even the plateau insinuated in Fig. 3(a) for 3 C (cathode–anode distance) is found in Fig. 8(b).

Fig. 9(a) shows in silico pH front tracking profiles for 5 and 10 mA, revealing that the front scales in time as $t^{0.601}$. This result is very well correlated with the in vitro agar measurements from Fig. 5(a). Fig. 9(b) shows in silico pH profiles for the same currents revealing a pH plateau in the middle of the distance cathode–anode mimicking the situation previous to the mixing of a cathodic alkaline pH front with an anodic acidic front, just as in the experimental measurements presented in Fig. 5(b).

Fig. 10(a) shows in silico electrostatic potential variations vs time for 5 and 10 mA, revealing that the voltage drop in the cell

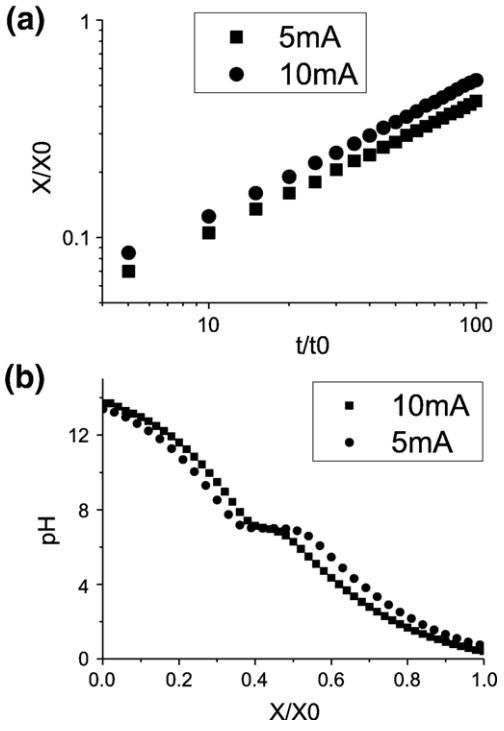

Fig. 9. Simulated pH front tracking (a) and simulated pH profiles vs distance cathode–anode (b). All plots made for 5 and 10 mA at t=600 (x_0=3 cm and t_0=1 s).

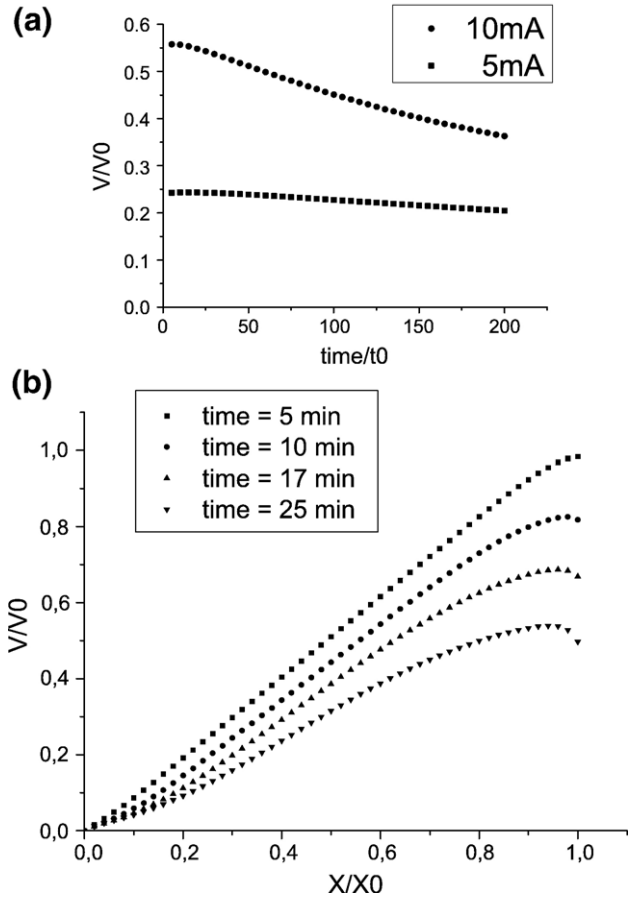

Fig. 10. Simulated electrostatic potential in the cell vs time for 5 and 10 mA (a); simulated electrostatic potential in the cell vs distance for different Coulomb dosages (b);(x_0=3 cm, t_0=1 s and V_0=1 V).

decreases in time and is more pronounced for higher electric currents. This is because resistance decreases in time due to the increase in H^+ and OH^- ions, as observed in the experiments of Fig. 6. Fig. 10(b) shows the in silico electrostatic potential drop vs distance cathode–anode, for different Coulomb dosages.

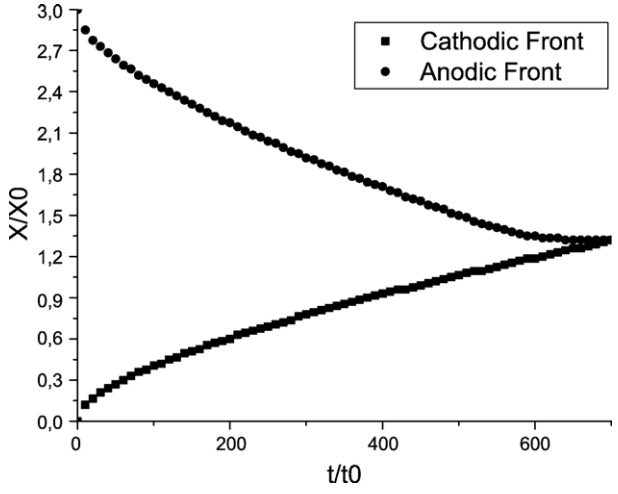

Fig. 11. Simulated Cl^- (a) and Na^+ (b) concentrations vs cathode–anode distance, for different Coulomb dosages (x_0=3 cm and $C_0=10^{-7}$ mol/dm^3).

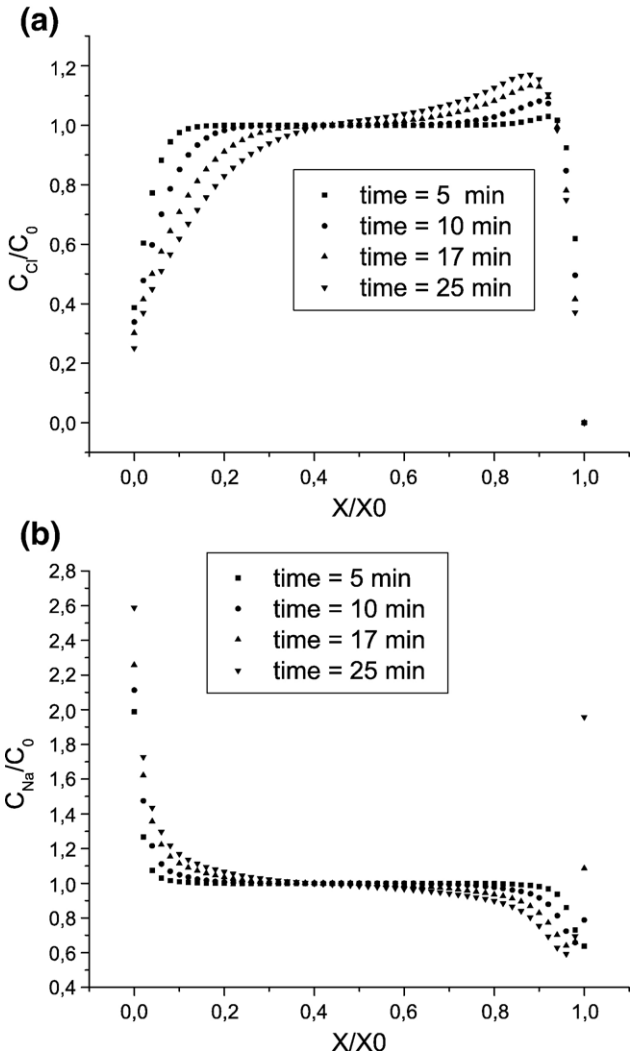

Fig. 12. Simulated Cl^- (a) and Na^+ (b) concentrations vs cathode–anode distance, for different Coulomb dosages (x_0=3 cm and $C_0=10^{-7}$ mol/dm^3).

Fig. 11 shows in silico cathodic OH^- and anodic H^+ pH front trajectories under galvanostatic conditions. As seen in the figure, the cathodic front reaches the anodic front at a distance of ≈1.4 which approximates the theoretical relation between H^+/OH^-. It can also be shown, by comparison of cathodic fronts from Figs. 11 (in a log–log scale) and 5(a) that they yield a very good correlation. These results show the ability of the in silico model for describing front interaction.

Finally, Fig.12(a) and (b) show simulated Cl^- and Na^+ concentration profiles vs cathode–anode distance for different Coulomb dosages. The model describes correctly the Cl^- and Na^+ spatial concentration variations expected in this sort of experiments(see [37] for details).

5. Discussion

To organize the discussion of the results of the combined methodology presented, that is, in vivo, in vitro and in silico modeling (VVS), first experimental results are analyzed and compared among themselves to address experimental model

coherence; then experiments are compared with simulations to integrate results in a unified theoretical framework and show VVS coherence, and finally, some general conclusions are drawn.

5.1. Comparing in vivo and in vitro experiments

The in vivo EChT measurements (Fig. 1) reveal that the macroscopic necrotic area around the anode, defined by an almost spherical colored zone, scales linearly with the Coulomb dosage. Fig. 2 reveals that from almost neutral values at the periphery the pH profile falls to zero at the anode. Concomitantly, the transport of water, from anode to cathode, produces a severe dehydration in the tissue around the anode and a prominent oedema at the cathode.

The cathode–anode pH profiles for both collagen (Fig. 3) and agar (Fig. 5(b)) in vitro measurements are strongly correlated: extreme pH values at the electrodes, separated by a plateau region (for a particular Coulomb dosage, e.g. 3 C). Both types of gels present a mesh-structure but differ mainly in their biochemical composition, being the agar gel a carbohydrate polymer and the collagen gel a protein-based one. This could imply some important differences for EChT treatment, including the fact that proteins denaturalize in conditions of extreme temperature or pH changes.

Anode–periphery pH profiles for in vivo and in vitro modeling follow the same trends showing model coherence: from neutral values at the periphery towards extremely acidic values at the anode. Although we do not have in vivo anode–cathode and cathode–periphery pH profiles, it is expected that they might be well correlated to those found in vitro. The dehydration and hydration at the anode and cathode, respectively, observed in the vivo modeling, was also observed in the in vitro collagen type I modeling, albeit much more attenuated. In both cases, this phenomenon might be due to the presence of electro-osmosis.

The in vitro EChT agar modeling allows the tracking in time of the alkaline pH front area around the cathode (defined by an almost spherical colored zone). The analysis reveals its scaling in time as $t^{1/2}$, a characteristic of diffusive transport. This fact indicates that convection is essentially suppressed by the high viscosity of the gel employed.

Although we do not have in vivo necrotic front evolution measurements, results from in vitro agar modeling suggest that they might scale in time as in Fig. 5(a). Also, agar voltage drop evolution in time (Fig. 6(a)) and the chlorine front tracking (Fig. 6(b)) suggest a close correlation with in vivo modeling, that is, the tissue resistance decrease in time and the chlorine front tracking is governed mainly by diffusion. Clearly, further measurements are needed before these facts can be proven to be correct.

5.2. Comparing in silico with in vivo and in vitro modeling

Comparing in silico Fig. 7 with in vivo Fig. 2 reveals that the predicted values are well correlated with the real ones: that is, near the anode pH concentration goes to zero while at the periphery approaches nearly neutral values. The slight differences in pattern observed are not surprising as we do not expect to have close agreement at this stage on the grounds of the crude approximation made with the in silico model.

Comparing in silico with in vitro, whether collagen or agar modeling, reveals that the predicted pH profiles are strongly correlated to the experimental ones. For instance, the spatial pH pattern predicted in Fig. 8 is close to the ones presented in Fig. 3 or Fig. 5(b). Comparison of Fig. 9(a) with Fig. 5(a) reveals that the time scale of the in silico modeling is slightly higher. This is perhaps due to an increment of the migration effect in the in silico model because of the use of constant mobility values rather than ionic strength dependant ones, as observed in the experiments. Comparing Fig. 10(a) with Fig. 6(a) reveals that the in silico potential drop in the cell is consistently higher than in the in vitro one, though the trend in time is close. Again, the different mobilities involved may also play a role in this discrepancy.

Comparison of pH anodic profiles from (Figs. 2, 3 (right column) and 7), reveals good correlation and thus, in vivo, in vitro and in silico, i.e. VVS, model coherence.

The in silico results presented in Figs. 10(b),11 and 12 showing the spatial potential drop variation, the anodic front trajectory, and the spatial chlorine and sodium concentration variations, respectively, do not have in vivo nor in vitro experimental measurements to compare with, though it is expected that they might be well correlated. Again, more experiments are needed to confirm this point.

6. Conclusions

In summary, with extreme caution our results suggest that the effects of EChT treatment on a human tumor might be correlated with those found in the triple modeling approach: extremely alkaline and acidic values at the cathode and anode respectively, recovering the neutral values not far from the electrodes. The tracking of the pH and necrotic fronts might have a time scaling close to $t^{1/2}$ indicating a diffusion-controlled ion transport. Moreover, the 1-D pH simulation allows the introduction of an imaginary 3-D view of the pH distribution along the cathode anode axis as follows. By rotation of Fig. 8 around the abscissa it is possible to imagine a solid of revolution consisting in a succession (in the periphery–cathode–anode–periphery sense) of two hyperboloids, a cylinder, another hyperboloid and a paraboloid. Since the tumor roughly consists in a core of necrotic tissue surrounded by an spherical active cancer cell casket, apparently, for the success of the EChT therapy, the electrodes should be located in such a way as to avoid the superposition of the biological pH strip resulting from the EChT treatment with the active zone of the tumor.

The present authors are aware of the crude approximations made in the extrapolation to human tumors made with the VVS methodology. Nevertheless, it is claimed that the VVS methodology presented here is a powerful tool allowing a complementary and thus richer multidisciplinary view of this complex problem while assuring that experimental and/or numerical artifacts are more easily detected. Furthermore, it is believed that the VVS results presented here will have significant implications in the description and understanding of tumor destruction by EChT and in a future design of optimal operative conditions and dose planning of this kind of therapy.

Acknowledgements

We thank anonymous referees for their valuable comments. L. C., G. G., G. M., F. M. and C. S. are investigators at the Consejo Nacional de Investigaciones Científicas y Técnicas (CONICET). C. S. has a fellowship from the Agencia Nacional de Promoción Científica y Técnica (ANPCyT). A. S. is partially supported by University of Buenos Aires (UBA). P. T. has a fellowship from CONICET. This work was partially supported by grants from UBA-CyT X122/04, ANPCyT: PICTR 184, CONICET: PIP 379/98 and Microsoft RFP2006 Digital Inclusion in Health and Higher Education Project.

References

[1] E. Nilsson, H. von Euler, J. Berendson, A. Thorne, P. Wersall, I. Naslund, A. Lagerstedt, K. Narfstrom, J. Olsson, electrochemical treatment of tumours, Bioelectrochemistry 51 (2000) 1–11.
[2] B. Nordenstrom, Biologically Closed Electrical Circuits: Clinical, Experimental and Theoretical Evidence for an Additional Circulatory System, Nordic Medical Publications, Stockholm, Sweeden, 1983.
[3] B. Nordenstrom, Electrochemical treatment of cancer i: variable response to anodic and cathodic fields, American Journal of Clinical Oncology 12 (6) (1989) 530–536.
[4] Y. Xin, Organization and spread of electrochemical therapy (EChT) in china, European Journal of Surgery. Supplement 574 (1994) 25–30.
[5] Y. Xin, The clinical advance in application of EChT within the past ten years, Preprints from the 2nd international symposium on electrochemical treatment (1998) 81–92.
[6] D. Miklavcic, G. Sersa, S. Novakovic, S. Rebersek, Tumor bioelectric potential and its possible exploitation for tumor growth retardation, Journal of Bioelectricity 9 (2) (1990) 133–149.
[7] D. Miklavcic, G. Sersa, M. Kryzanowski, S. Novakovic, F. Bobanovic, R. Golouh, L. Vodovnik, Tumor treatment by direct electric current: tumor temperature and pH, electrode material and configuration, Bioelectrochemistry and Bioenergetics Book Chapter, vol. 52, 1993, pp. 417–427.
[8] G. Sersa, D. Miklavcic, The feasibility of low level direct current electrotherapy for regional cancer treatment, Regional Cancer Treatment 6 (1) (1993) 31–35.
[9] D. Miklavcic, A. Fajgelj, G. Sersa, Tumour treatment by direct electric current: electrode material deposition, Bioelectrochemistry and Bioenergetics 35 (1–2) (1994) 93–97.
[10] G. Sersa, S. Novakovic, D. Miklavcic, Potentiation of bleomycin antitumor effectiveness by electrotherapy, Cancer Letters 69 (2) (1993) 81–84.
[11] H. von Euler, K. Strahle, A. Thorne, G. Yongqing, Cell proliferation and apoptosis in rat mammary cancer after electrochemical treatment (EChT), Bioelectrochemistry 62 (2004) 57–65.
[12] L. Cabrales, L. Luna, La electroterapia: una alternativa terapéutica para el tratamiento de tumores, Revista Cubana de Medicina 42 (6) (2003).
[13] H. Ciria, D. Lpez, La electroquimioterapia: una nueva alternativa teraputica en la oncologa, Revista Cubana de Oncologa 17 (3) (2001) 188–194.
[14] H. Ciria, M. Quevedo, L. Cabrales, R. Bruzon, M. Salas, O. Pena, T. Gonzlez, D. Lpez, J. Flores, Antitumor effectiveness of different amounts of electrical charge in Ehrlich and fibrosarcoma sa-37 tumors, BMC Cancer 4 (1) (2004) 87.
[15] E. Neumann, K. Rosenheck, Permeability changes induced by electric impulses in vesicular membranes, Journal of Membrane Biology 10 (1972) 279.
[16] L. Mir, M. Belehradek, C. Domenge, S. Orlowski, B. Poddevin, J. Belehradek Jr., G. Schwaab, B. Luboinski, C. Paoletti, Electrochemotherapy, a novel antitumor treatment: first clinical trial, Comptes Rendus de l'Academie des Sciences. Serie III, Sciences de la vie 313 (13) (1991) 613–618.
[17] Z. Rudolf, B. Stabuc, M. Cemazar, D. Miklavcic, L. Vodovnik, G. Sersa, Electrochemotherapy with bleomycin. The first clinical experience in malignant melanoma patients, Radiology and Oncology 29 (3) (1995) 229–235.
[18] G. Sersa, The state-of-the-art of electrochemotherapy before the scope study; advantages and clinical uses, European Journal of Cancer. Supplement 4 (11) (2006) 52–59.
[19] M. Knowles, S.P., Introduction to the Cellular and Molecular Biology of Cancer, 4th edOxford University Press, Oxford, 2005 GB.
[20] P. Netti, D. Berk, M. Swartz, A. Grodzinsky, R. Jain, Role of extracellular matrix assembly in interstitial transport in solid tumors, Cancer Research 60 (2000) 2497–2503.
[21] S. Ramanujan, A. Pluen, T. McKee, E. Brown, Y. Boucher, R. Jain, Diffussion and convection in collagen gels: implications for transport in the tumor interstitium, Biophysics Journal 83 (3) (2002) 1650–1660.
[22] L. Preziosi, Cancer Modelling and Simulation, CHAPMAN & HALL/CRC, London, UK, 2003.
[23] L.T. Baxter, R.K. Jain, Transport of fluid and macromolecules in tumors. i. Role of interstitial pressure and convection, Microvascular Research 37 (1) (1989) 77–104.
[24] L.T. Baxter, R.K. Jain, Transport of fluid and macromolecules in tumors. ii. Role of heterogeneous perfusion and lymphatics, Microvascular Research 40 (2) (1990) 246–263.
[25] L.T. Baxter, R.K. Jain, Transport of fluid and macromolecules in tumors: Iii. role of binding and metabolism, Microvascular Research 41 (1) (1991) 5–23.
[26] L.T. Baxter, R.K. Jain, Transport of fluid and macromolecules in tumors. iv. A microscopic model of the perivascular distribution, Microvascular Research 41 (2) (1991) 252–272.
[27] E. Nilsson, J. Berendson, E. Fontes, Development of a dosage method for electrochemical treatment of tumours: a simplified mathematical model, Bioelectrochemistry and Bioenergetics 47 (1998) 11–18.
[28] E. Nilsson, J. Berendson, E. Fontes, Electrochemical treatment of tumours: a simplified mathematical model, Journal of Electroanalytical Chemistry 460 (1999) 88–99.
[29] E. Nilsson, J. Berendson, E. Fontes, Impact of chlorine and acidification in the electrochemical treatment of tumours, Journal of Applied Electrochemistry 30 (12) (2000) 1321–1333.
[30] E. Nilsson, E. Fontes, Mathematical modeling of physicochemical reactions and transport processes occurring around a platinum cathode during the electrochemical treatment of tumours, Bioelectrochemistry 53 (2001) 213–224.
[31] G. Marshall, P. Mocskos, A growth model for ramified electrochemical deposition in the presence of diffusion, migration and electroconvection, Physical Review E, Statistical, Nonlinear, and Soft Matter Physics 55 (1997) 549.
[32] G. Marshall, P. Mocskos, H.L. Swinney, J.M. Huth, Buoyancy and electrical driven convection, Physical Review E, Statistical, Nonlinear, and Soft Matter Physics 59 (1999) 2157.
[33] S. Dengra, G. Marshall, F. Molina, Front tracking in thin-layer electrodeposition, Journal of the Physical Society of Japan 69 (3) (2000) 963–971.
[34] G. Gonzalez, G. Marshall, F.V. Molina, S. Dengra, M. Rosso, Viscosity effects in thin-layer electrodeposition, Journal of The Electrochemical Society 148 (7) (2001) C479–C487.
[35] G. Gonzalez, G. Marshall, F. Molina, S. Dengra, Transition from gravito- to electroconvective regimes in thin-layer electrodeposition, Physical Review. E, Statistical, Nonlinear, and Soft Matter Physics 65 (5) (2002) 051607.
[36] G. Marshall, E. Mocskos, F.V. Molina, S. Dengra, Three-dimensional nature of ion transport in thin-layer electrodeposition, Physical Review E, Statistical, Nonlinear, and Soft Matter Physics 68 (2) (2003) 021607.
[37] G. Marshall, F. Molina, A. Soba, Ion transport in thin cell electrodeposition: modelling three-ion electrolytes in dense branched morphology under constant voltage and current conditions, Electrochimica Acta 50 (2005) 3436–3445.
[38] R. Lemberg, J. Legge, Haemain Compounds and Bile Pigments, Interscience Publishers, Inc., New York, 1949.
[39] L. Samuelsson, T. Olin, N. Berg, Electrolytic destruction of lung tissue in the rabbit, Acta Radiologica. Diagnosis 21 (4) (1980) 447–454.
[40] A. Pluen, Y. Boucher, S. Ramanujan, T. McKee, T. Gohongi, E. di Tomaso, E. Brown, Y. Izumi, R. Campbell, D. Berk, R. Jain, Role of tumor–host interactions in interstitial diffusion of macromolecules: cranial vs subcutaneous tumors, Proceedings of the National Academy of Sciences 98 (8) (2001) 4628–4633.